A&A 394, L31–L34 (2002)
DOI: 10.1051/0004-6361:20021380

Astronomy & Astrophysics

The kinematic relationship between disk and jet in the DG Tauri system

L. Testi[1], F. Bacciotti[1], A. I. Sargent[2], T. P. Ray[3], and J. Eislöffel[4]

[1] Osservatorio Astrofisico di Arcetri, INAF, Largo E. Fermi 5, 50125 Firenze, Italy
[2] California Institute of Technology, MS 105-24, Pasadena, CA 91125, USA
[3] Dublin Institute for Advanced Studies, 5 Merrion Square Dublin 2, Ireland
[4] Thüringer Landessternwarte Tautenburg, Sternwarte 5, 07778 Tautenburg, Germany

Received 21 August 2002 / Accepted 20 September 2002

Abstract. We present high angular resolution millimeter wavelength continuum and ^{13}CO(2–1) observations of the circumstellar disk surrounding the T Tauri star DG Tauri. We show that the velocity pattern in the inner regions of the disk is consistent with Keplerian rotation about a central 0.67 $M_{\odot}$ star. The disk rotation is also consistent with the toroidal velocity pattern in the initial channel of the optical jet, as inferred from HST spectra of the first de-projected 100 AU from the source. Our observations support the tight relationship between disk and jet kinematics postulated by the popular magneto-centrifugal models for jet formation and collimation.

Key words. circumstellar matter – jets and outflows – stars: formation – stars: individual: DG Tauri

1. Introduction

The interplay between accretion and ejection of matter is believed to be a crucial element in the formation of stars. In particular, stellar jets may contribute substantially to the removal of excess angular momentum from the system, thereby allowing the central star to accrete to its final mass (e.g. Eislöffel et al. 2000; Königl & Pudritz 2000; Shu et al. 2000). Most of the proposed models invoke the simultaneous action of magnetic and centrifugal forces in a rotating star/disk system threaded to open magnetic field lines. Even if widely accepted, these models have not yet been tested observationally on the launching scale (a few AU from the star), although this may be possible with the coming generation of interferometers. On much larger scales, there is some evidence for the requisite relationship between the jet and envelope kinematics in the HH 212 protostellar system (Davis et al. 2000). Hints of rotation are seen in the H_2 jet knots at 2×10^3 to 10^4 AU from the powering source; the sense of rotation is the same as that of the flattened envelope detected in NH_3 VLA observations (Wiseman et al. 2001). Although encouraging, these measurements probe regions too far from the central source to allow detailed comparison between the disk and jet kinematics.

Protostellar disk/jet systems are too embedded to probe the jet close to the launching region with current techniques which rely on optical and near infrared observations. Moreover, the kinematics of disk/envelope systems may encompass both rotational and infall motions, hampering tests of disk-jet interaction models. Optically visible T Tauri stars, which have associated disks but little remnant envelopes, are much more suitable candidates for such studies.

The optical jet from the T Tauri star DG Tauri has been extensively studied at high resolution in recent years and displays properties that are in general agreement with magneto-centrifugal models for jet-launching (Dougados et al. 2000; Bacciotti et al. 2000, 2002). The latter studies showed that the flow appears to have an onion-like kinematic structure, with the faster and more collimated flow continuously bracketed in a wider and slower one. The flow becomes gradually denser and more excited from the edges toward the axis. The mass loss rate in the flow is about one tenth of the estimated mass accretion rate through the disk (Bacciotti et al. 2000). Even more interestingly, for the spatially resolved flow component at moderate velocity (peaked at $-70\,\mathrm{km\,s^{-1}}$) systematic offsets in the radial velocity of the lines have been found in pairs of slits symmetrically located with respect to the jet axis (Bacciotti et al. 2002). If these results are interpreted as rotation, then the jet is rotating clockwise (looking toward the source) with average toroidal velocities of about 10–15 $\mathrm{km\,s^{-1}}$, in the region probed by the observations (i.e. 10–50 AU from both the star and jet axis). All of these properties, including the implied velocities and angular momentum fluxes are in the range predicted by the models, assuming a central star mass of 0.67 $M_{\odot}$

Send offprint requests to: L. Testi, e-mail: lt@arcetri.astro.it

(Hartigan et al. 1995). The kinematic properties of the material surrounding the star are of crucial importance in further establishing if the models apply.

DG Tauri is known to be surrounded by a circumstellar disk (Beckwith et al. 1990; Kitamura et al. 1996a; Dutrey et al. 1996). Previous interferometric observations of the molecular component of the system (Sargent & Beckwith 1994; Kitamura et al. 1996b, hereafter KKS) could not identify a clear signature for rotation around the central object. These relatively low-resolution (4–5″), ^{13}CO(1–0) observations could not disentangle the kinematics of the circumstellar disk from the outflow and the outer envelope velocity fields. In fact, the environment of the star on large scales appears to be dominated by outflow motions, possibly due to the interaction between the outer regions of the disk and the stellar wind (KKS). In contrast, the inner portion of the disk, closer to the jet launching region, is expected to display a Keplerian rotation pattern. We have carried out new, higher-resolution millimeter wavelength observations of the ^{13}CO(2–1) transition toward the DG Tauri system with the aim of distinguishing the velocity field close to the star and ascertaining if it is consistent with that expected for Keplerian rotation and to check that the disk and jet rotate in the same sense.

2. Observations and results

Millimeter wavelength interferometric observations of the DG Tauri system was performed using the Owens Valley Radio Observatory (OVRO) mm-array located near Big Pine, California, between Oct. 1999 and Dec. 2001. The six 10.4 m dishes were deployed in configurations that provided baselines from 15 to 240 m. Continuum observations centered at ∼220 and ∼108 GHz used an analog correlator with a total bandwidth of 2 GHz. The digital correlator was configured to observe the ^{13}CO(2–1) transition with 0.125 MHz resolution over an 8 MHz band (0.17 and 11 km s^{-1}, respectively). Frequent observations of 0528+134 were used to perform phase and gain calibration. The passband calibration was obtained by observing 3C 273, 3C 454.3 and/or 3C 84. The flux density scale was derived by observing Neptune and/or Uranus, and the calibration uncertainty is expected to be ∼20%. All calibration and data editing used the MMA software package (Scoville et al. 1993). Calibrated (u, v) data were then loaded into the AIPS and/or GILDAS packages for imaging, deconvolution and analysis. Continuum maps and line cubes were produced using natural weighting of the (u, v) data, and smoothed to a spectral resolution of 0.5 km s^{-1}, unless specifically noted. The synthesized beam full width at half maximum is 1.″7×1.″4. Continuum subtraction was performed on the dirty images before deconvolution using channels at the edge of the band.

2.1. Continuum maps

We detect unresolved continuum emission from DG Tauri at both 1.3 and 2.7 mm. The peak position is the same at both wavelengths, $\alpha(2000) = 04^{\rm h}27^{\rm m}04\overset{\rm s}{.}66$ $\delta(2000) = 26°06'16\overset{''}{.}3$, in agreement with previous measurements (e.g. Kitamura et al. 1996a; KKS). The total flux density is 215 mJy at 222 GHz and 55 mJy at 108 GHz. Within calibration uncertainties, the 3 mm value agrees with earlier interferometer measurements (KKS; Dutrey et al. 1996; Looney et al. 2000) but the 1.3 mm value is a factor of two lower than the single dish flux (Beckwith et al. 1990), probably because of spatial filtering by the interferometer. If we assume optically thin emission from dust grains at $T \sim 40$ K and a dust opacity coefficient $k_\nu = k_{230\,\rm GHz} \times (\nu/230\,\rm GHz)^\beta$, with $k_{230\,\rm GHz} = 0.01$ (Hildebrand 1983, including a gas to dust ratio of 100 by mass), and $\beta \sim 0.5$ (Beckwith & Sargent 1991), our measurements imply a total mass of ∼0.04 $M_\odot$, consistent with previous estimates.

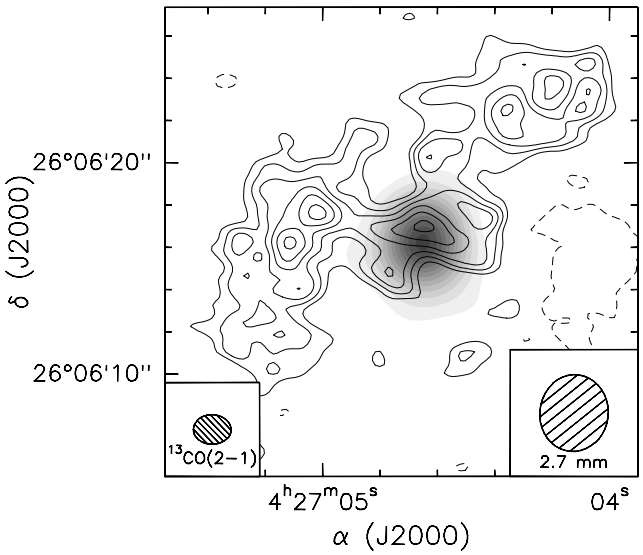

Fig. 1. OVRO ^{13}CO(2–1) integrated intensity map (contours) overlaid on the 2.7 mm continuum image (greyscale).

2.2. Line maps

In Fig. 1 we show the ^{13}CO(2–1) integrated intensity map overlaid on the 2.7 mm continuum image. Our observations are sensitive only to the compact features of the emission and resolve out most of the extended core emission seen in the KKS maps. In spite of the filtering by the interferometer, most of the ^{13}CO(2–1) emission is not concentrated in the inner regions of the system close to the position of the optical star. The velocity pattern exhibited by this extended gaseous component has been interpreted by KKS as due to an expanding disk-like structure, possibly the outer edge of the disk that is being dispersed by the stellar wind. Our higher angular resolution map is in good agreement with their interpretation. In this paper however, we will focus on the inner regions of the disk.

In Fig. 2 we show ^{13}CO(2–1) channel maps (0.5 km s^{-1} resolution) of the central ∼12″ region centered on the continuum peak position (marked by a cross). The core of the line ($v_{\rm LSR}$ = 5.0–7.0 km s^{-1}) is dominated by the poorly imaged extended structure discussed above. Note that the central velocity channels may also be affected by self-absorption due to cold foreground gas (Schuster et al. 1993). By contrast, the higher velocity wings, corresponding to the leftmost three blue and red channels, display compact emission arising from

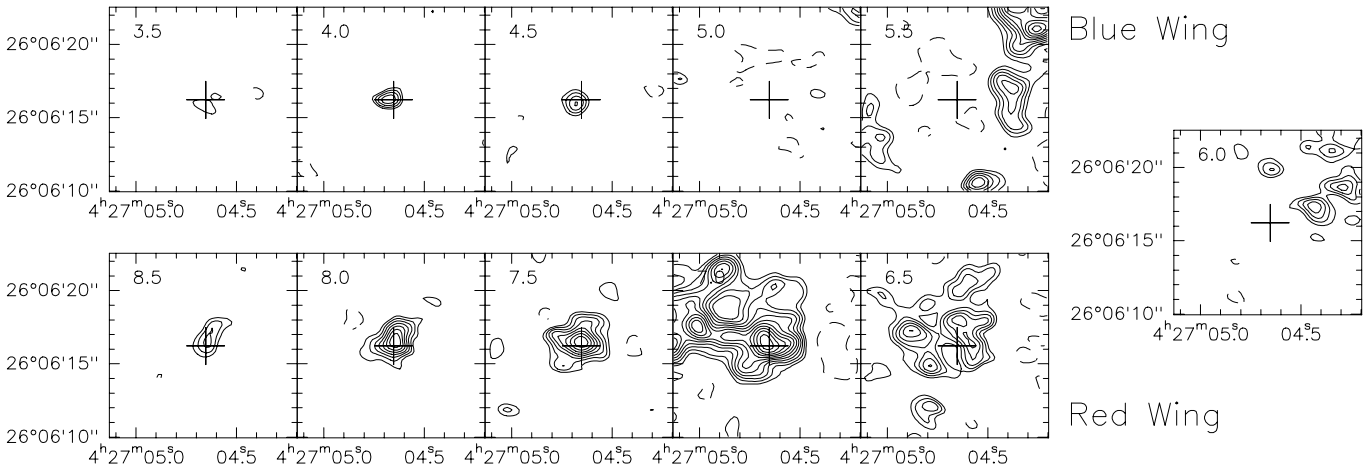

Fig. 2. ^{13}CO(2–1) channel maps. Top panels: blue wing; bottom panels: red wing. Each panel is labelled with the appropriate velocity ($v_{\rm LSR}$ in km s^{-1}). The cross marks the position of the 1.3 mm continuum peak. Contour levels start at 3σ and are spaced by 1σ = 60 mJy/beam. The central velocity of the system is assumed to be ~6.0 km s^{-1} (rightmost, isolated panel).

the inner disk. The maps show that the emission peak in the blue channels is shifted toward the south-east with respect to the continuum peak, while in the red channels it is shifted to the north-west. In order to emphasize this velocity gradient, in Fig. 3 we show the wing emission integrated over the ranges $v_{\rm LSR}$ = 3.5–4.5 km s^{-1} (blue wing) and 7.5–8.5 km s^{-1} (red wing). These maps were obtained with a robust weighting of the (u, v) data and the resulting angular resolution is $1\farcs4 \times 1\farcs0$. The red and blue wing emission peaks on opposite sides of the continuum, which is assumed to trace the stellar position (see also KKS), and is aligned along a line approximately perpendicular to the observed direction of the optical jet (PA ~ 226°, marked with a thick line in Fig. 3).

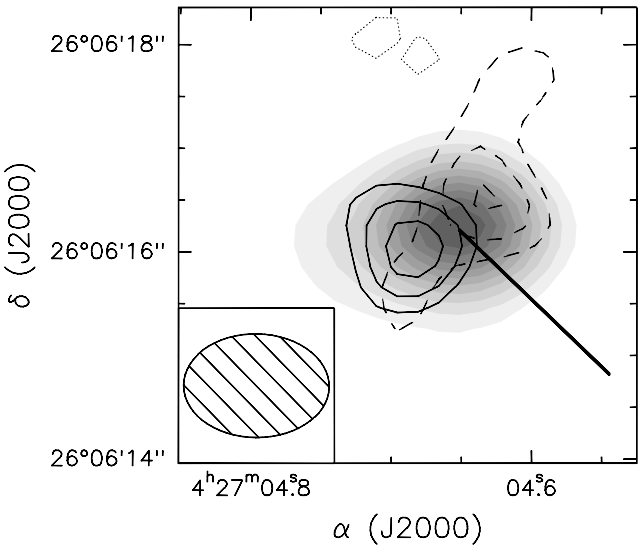

Fig. 3. ^{13}CO(2–1) wing maps (contours) overlaid on the 1.3 mm continuum image (greyscale). Blue and red wing are shown as solid and dashed contours, respectively. Contour levels start at 3σ and are spaced by 1σ, dotted lines show negative contours. The thick solid line indicates the direction and extent of the initial segment of the optical jet studied by Bacciotti et al. (2002).

3. Discussion

The prime goal of this study was to investigate the velocity pattern in the inner regions of the DG Tauri disk and to relate it to the velocity pattern detected at the base of the optically visible jet by Bacciotti et al. (2002). The channel and wing maps of Figs. 2 and 3 indeed show a velocity gradient across the inner regions of the circumstellar disk. If interpreted as rotation within a disk the axis of which coincides with the jet axis, the direction of the gradient is consistent with the sense of rotation inferred for the jet.

Due to the contamination of the poorly imaged external regions of the disk, and self-absorption, it is not possible to study the kinematics of the inner disk using the line core within 1 km s^{-1} from the systemic velocity, assumed to be 5.8 km s^{-1} (KKS). In particular, there can be no detailed comparison of the observed velocity patterns with Keplerian rotation models such as those undertaken by Koerner et al. (1993), Guilloteau & Dutrey (1994) and Mannings et al. (1997). Nevertheless, in Fig. 4 position-velocity diagrams along directions parallel and perpendicular to the jet suggest that, along the disk major axis ($\Delta_\perp$), higher absolute velocity (with respect to the systemic velocity) peaks are located closer to the star, while the lower absolute velocities peak further away. Moreover, blue velocities systematically peak to the south-east and red velocities peak to the north-west of the stellar position. This behaviour is qualitatively consistent with Keplerian rotation in the inner regions of the disk. A more quantitative comparison with the expected line-of-sight velocities for a disk surrounding DG Tauri is shown in Fig. 4, bottom panel. The theoretical curves in the figure were computed for a central star with mass $M_\star$ = 0.67 $M_\odot$ (Hartigan et al. 1995), and an inclination from the line of sight of 38° (Eislöffel & Mundt 1998); these are the parameters adopted by Bacciotti et al. (2002) to check the rotational hypothesis for the jet. The dotted lines include an uncertainty in these parameters of ±0.25 $M_\odot$ and ±15°. The observed

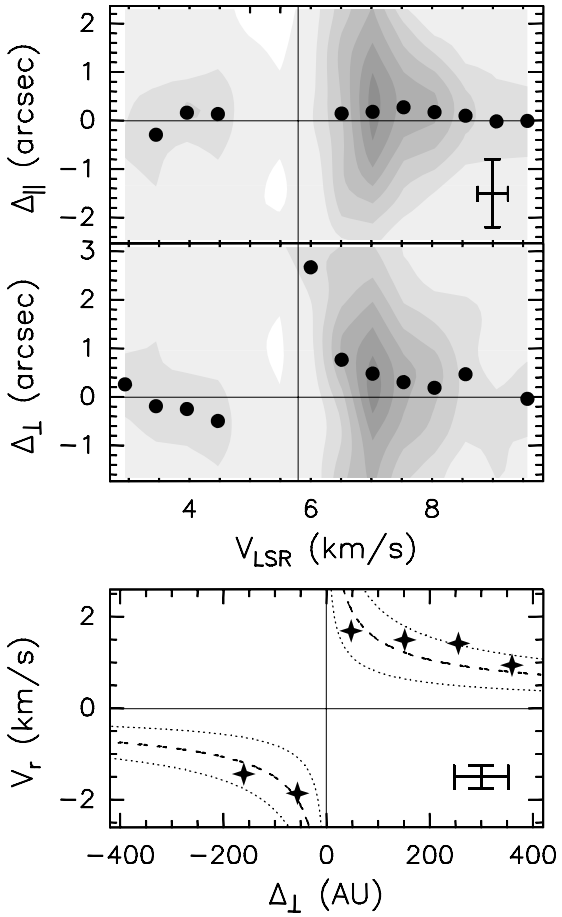

Fig. 4. Top panels: ^{13}CO(2–1) position-velocity diagrams parallel (top) and perpendicular (bottom) to the jet axis. The crosses mark the intensity averaged position at each velocity, computed only if the emission is above 3σ. Errorbars in the top panel show the velocity and spatial resolutions. The thin lines mark the core average velocity (5.8 km s^{-1}) and the position of the continuum source. Bottom panel: intensity averaged line of sight velocities in the first and third quadrant of the lower position-velocity diagram, averaged every 0.″75 (105 AU). The dashed line marks the expected line of sight velocity across a Keplerian disk with the axis inclined by 38° from the line of sight and orbiting about a 0.67 $M_\odot$ star at a distance of 140 pc from the Sun. The dotted lines show the range of variation of the Keplerian disk predictions for a maximum uncertainty of ±15° in the inclination angle and ±0.25 $M_\odot$ in the stellar mass.

velocity pattern in the inner regions of the disk is in excellent agreement with the model predictions. A more detailed comparison, including the complete derivation of the disk rotation from molecular line observations, will require higher angular resolution and more sensitive observations of optically thinner transitions, such as C^{18}O(2–1), which are possibly less affected by the external regions of the disk/envelope.

Summarizing our results, we have shown for the first time that the disk kinematics in a young T Tauri system are in qualitative and quantitative agreement with the velocity pattern at the base of the jet. In other words, the simultaneous and kinematically consistent rotation of disk and jet postulated by the popular magneto-centrifugal models has been observationally inferred for the first time for the region within ~200 AU from the central source.

Acknowledgements. The OVRO mm array is supported by NSF grant AST-99-81546, research on young stars and disks is also supported by the *Norris Planetary Origins Project* and NASA *Origins of Solar Systems* program (grant NAG5–9530). We thank the referee, Chris Davis, for comments that improved the presentation of our results.

References

Bacciotti, F., Mundt, R., Ray, T. P., et al. 2000, ApJ, 537, L49
Bacciotti, F., Ray, T. P., Mundt, R., Eislöffel, J., & Solf, J. 2002, ApJ, 576, 222
Beckwith, S. V. W., Sargent, A. I., Chini, R. S., & Güsten, R. 1990, AJ, 99, 924
Beckwith, S. V. W., & Sargent, A. I. 1991, ApJ, 381, 250
Davis, C. J., Berndsen, A., Smith, M. D., Chrysostomou, A., & Hobson, J. 2000, MNRAS, 314, 241
Dougados, C., Cabrit, S., Lavalley, C., & Ménard, F. 2000, A&A, 357, L61
Dutrey, A., Guilloteau, S., Duvert, G., et al. 1996, A&A, 309, 493
Eislöffel, J., & Mundt, R. 1998, AJ, 115, 1554
Eislöffel, J., Mundt, R., Ray, T. P., & Rodríguez, L. F. 2000, in Protostars and Planets IV, ed. V. Mannings, A. P. Boss, & S. S. Russell (Tucson: University of Arizona Press), 815
Guilloteau, S., & Dutrey, A. 1994, A&A, 291, L23
Hartigan, P., Edwards, S., & Ghandour, L. 1995, ApJ, 452, 736
Hildebrand, R. H. 1983, QJRAS, 24, 267
Kitamura, Y., Kawabe, R., & Saito, M. 1996a, ApJ, 465, L137
Kitamura, Y., Kawabe, R., & Saito, M. 1996b, ApJ, 457, 277 (KKS)
Koerner, D. W., Sargent, A. I., & Beckwith, S. V. W. 1993, Icarus, 106, 2
Königl, A., & Pudritz, R. E. 2000, in Protostars and Planets IV, ed. V. Mannings, A. P. Boss, & S. S. Russell (Tucson: University of Arizona Press), 759
Looney, L. W., Mundy, L. G., & Welch, W. J. 2000, ApJ, 529, 477
Mannings, V., Koerner, D. W., & Sargent, A. I. 1997, Nature, 388, 555
Sargent, A. I., & Beckwith, S. V. W. 1994, in IAU Coll. 140, Astronomy with Millimeter and Submillimeter Wave Interferometry, ed. M. Ishiguro, & W. J. Welch (San Francisco: ASP), 203
Shu, F. H., Najita, J. R., Shang, H., & Li, Z.-Y. 2000, in Protostars and Planets IV, ed. V. Mannings, A. P. Boss, & S. S. Russell (Tucson: University of Arizona Press), 789
Schuster, K. F., Harris, A. I., Anderson, N., & Russell, A. P. G. 1993, ApJ, 412, L67
Scoville, N. Z., Carlstrom, J. E., Chandler, C. J., et al. 1993, PASP, 105, 1482
Wiseman, J., Wootten, A., Zinnecker, H., & McCaughrean, M. J. 2001, ApJ, 550, L87